



Rayleigh wave tomography in the North Atlantic: high resolution images of the Iceland, Azores and Eifel mantle plumes

Sylvana Pilidou^{a,*}, Keith Priestley^a, Eric Debayle^b, Ólafur Gudmundsson^c

^a*Bullard Laboratories, University of Cambridge, United Kingdom*

^b*Ecole et Observatoire des Sciences de la Terre, Université Louis Pasteur, Strasbourg, France*

^c*Danish Lithosphere Centre, Copenhagen, Denmark*

Received 23 October 2003; accepted 9 September 2004

Available online 6 November 2004

Abstract

Presented in this paper is a high resolution S_v -wave velocity and azimuthal anisotropy model for the upper mantle beneath the North Atlantic and surrounding region derived from the analysis of about 9000 fundamental and higher-mode Rayleigh waveforms. Much of the dataset comes from global and national digital seismic networks, but to improve the path coverage a number of instruments at coastal sites in northwest Europe, Iceland and eastern Greenland was deployed by us and a number of collaborators. The dense path coverage, the wide azimuthal distribution and the substantial higher-mode content of the dataset, as well as the relatively short path-lengths in the dataset have enabled us to build an upper mantle model with a horizontal resolution of a few hundred kilometers extending to 400 km depth. Low upper mantle velocities exist beneath three major hotspots: Iceland, the Azores and Eifel. The best depth resolution in the model occurs in NW Europe and in this area low S_v -velocities in the vicinity of the Eifel hotspot extend to about 400 km depth. Major negative velocity anomalies exist in the North Atlantic upper mantle beneath both Iceland and the Azores hotspots. Both anomalies are, above 200 km depth, 4–7% slow with respect to PREM and elongated along the mid-Atlantic Ridge. Low velocities extend to the south of Iceland beneath the Reykjanes Ridge where other geophysical and geochemical observations indicate the presence of hot plume material. The low velocities also extend beneath the Kolbeinsey Ridge north of Iceland, where there is also supporting geochemical evidence for the presence of hot plume material. The low-velocity upper mantle beneath the Kolbeinsey Ridge may also be associated with a plume beneath Jan Mayen. The anomaly associated with the Azores extends from about 25°N to 45°N along the ridge axis, which is in agreement with the area influenced by the Azores Plume, predicted from geophysical and geochemical observations. Compared to the anomaly associated with Iceland, the Azores anomaly is elongated further along the ridge, is shallower and decays more rapidly with depth. The fast propagation direction of horizontally propagating S_v -waves in the Atlantic south of Iceland correlates well with the east–west ridge-spreading direction at all depths and changes to a direction close to NS in the vicinity of Iceland.

© 2004 Elsevier B.V. All rights reserved.

Keywords: Surface wave tomography; Azimuthal anisotropy; Mantle plumes; Iceland; Azores; Eifel; Mid-Atlantic Ridge

* Corresponding author. Tel.: +357 99 376862.

E-mail address: s_pilidou@yahoo.co.uk (S. Pilidou).

1. Introduction

The two major tectonic features of the North Atlantic Ocean are the mid-Atlantic Ridge and the oceanic plateau surrounding Iceland (Fig. 1). The volcanic edifice on which Iceland sits results from enhanced melting due to the interaction of the mid-Atlantic Ridge and the Iceland Plume (McKenzie,

1984; Sleep, 1990). While the crustal structure of Iceland has been intensely studied with a variety of geophysical methods (Bjarnason et al., 1993; Staples et al., 1997; Darbyshire et al., 2000a,b; Allen et al., 2002b), the width and depth extent of the plume core in the mantle beneath Iceland is controversial (e.g., Wolfe et al., 1997; Bijwaard and Spakman, 1999; Keller et al., 2000; Foulger et al., 2001), and very little

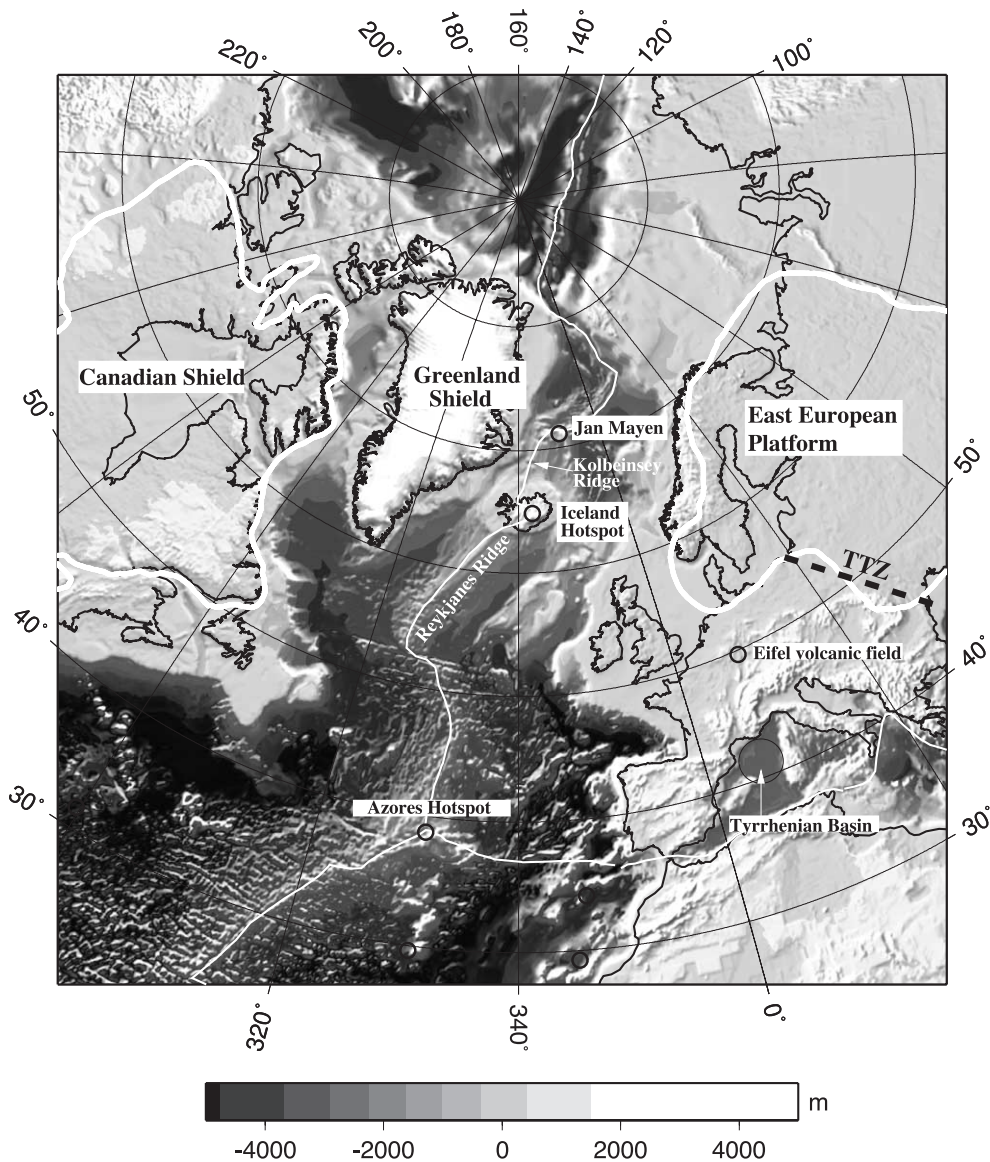


Fig. 1. Topography and bathymetry of the North Atlantic area. The thin solid white line defines the plate boundaries and the thick solid white lines refine the Canadian and East-European craton boundaries. The small black circles represent the locations of known hotspots (Sleep, 1990).

is known about the extent of the plume head in the upper mantle beneath the surrounding North Atlantic.

Early global tomographic studies produced images with too low resolution to resolve features possibly associated with hotspots in the North Atlantic. However, recent global models employing body wave data (e.g., Ritsema et al., 1999) clearly show low-velocity features in the uppermost mantle beneath the Iceland and Azores hotspots. Teleseismic body wave travel-time tomography has been used to argue for the existence beneath Iceland of both a continuous plume through the whole mantle (Bijwaard and Spakman, 1999), and a plume confined to the upper mantle (Foulger et al., 2001). Bijwaard and Spakman (1999) use a large P-wave arrival time dataset to derive a tomographic image beneath the North Atlantic, which shows a complex, low-velocity structure with numerous lateral branches extending from the upper mantle to the core-mantle boundary beneath most of the North Atlantic at the latitude of Iceland. Zhao (2001) invert P, PP, pP and PcP travel times and obtain a similar image. Shen et al. (1996, 1998) find the transition zone to be anomalously thin beneath Iceland and attribute this to hot material penetrating the transition zone from below. Helmberger et al. (1998) find evidence for an ultra-low-velocity anomaly in the D'' layer beneath the North Atlantic and suggest that this may be associated with a core-mantle boundary source of the Iceland Plume.

Travel time tomography studies using data collected on Iceland (e.g., Tryggvason et al., 1983; Wolfe et al., 1997; Foulger et al., 2001, Allen et al., 2002a) are consistent with a strong, about 200 km wide, low-velocity anomaly extending down to 400 km depth, the purported depth resolution limit of the seismic network, but there is no agreement on the shape of the low-velocity anomaly (Wolfe et al., 1997; Foulger et al., 2001). However, travel-time tomography studies using data collected on Iceland are hampered by the small aperture of the seismic network permitted by land-based seismographs and the poor distribution of regional earthquakes. For example, Keller et al. (2000) simulated a teleseismic body wave travel-time dataset for Iceland based on the observations of Wolfe et al. (1997) and show that, because of the relatively small aperture of the Icelandic seismic networks and the steeply arriving rays from the teleseismic sources, it is impossible to distinguish between a shallow, low-

velocity anomaly in the upper 200 km and a cylindrical low-velocity anomaly extending to greater depth, suggesting that the actual depth resolution of the network is less than 400 km.

Presented in this paper is a high resolution 3D shear-velocity and azimuthal anisotropy model for the upper mantle of the North Atlantic Ocean and surrounding region from surface wave tomography. Our primary interest is to obtain a high-resolution image of the entire extent of the Iceland Plume in the upper mantle. A similar, but much larger, dataset than Pilidou et al. (2004) is used and a slightly different analysis procedure is followed. Because S-wave velocities are particularly sensitive to temperature, S-wave speed maps are valuable for understanding thermal variations in the mantle. About 9000 multi-mode Rayleigh waveforms recorded over relatively short paths are used, thus minimizing artifacts in the tomographic model arising from off-great-circle path propagation. The dense path coverage, the wide azimuthal distribution, the substantial higher-mode content of the data and the short path-lengths have made it possible to build an upper mantle model for the North Atlantic with a horizontal resolution of a few hundred kilometers extending to 400 km depth.

2. Surface waveform fitting and tomography

The 3D upper mantle Earth model is constructed following a procedure similar to the two-step procedure used in a number of previous studies (e.g., Debayle and Kennett, 2000; Priestley and Debayle, 2003). Here, the specific details of the method as applied to this study of the North Atlantic are discussed; a complete discussion of various aspects of the waveform inversion technique and the tomography can be found in Montagner (1986), Cara and L ev eque (1987), L ev eque et al. (1991, 1998), Debayle (1999), and Debayle and Kennett (2000).

The automated version (Debayle, 1999) of the Cara and L ev eque (1987) waveform inversion technique is first used to determine a 1D path-average upper mantle velocity model from each observed Rayleigh waveform. This method uses secondary observables, which are built from the data by cross-correlation techniques, to minimize the problem of strong non-

linearity which characterizes the relation between the observed waveforms and the elastic parameters to be inverted for. The automated version of the (Cara and Lévêque, 1987) inversion code allows us to take advantage of the enormous volume of waveform data available to constrain the 3D upper mantle structure of the North Atlantic. It is, however, a very conservative procedure; after strict signal-to-noise ratio criteria initially applied on the data, each inversion is considered successful if the final model provides a good fit to both the secondary observables and the observed seismogram and if the inversion has converged towards a stable velocity model.

For both, the reference model used in determining the secondary observables and for the starting model in the inversion for the velocity structure a smooth version of PREM (Dziewonski and Anderson, 1981) is used for the mantle structure with a path-specific crustal model determined by averaging the crustal part of 3SMAC (Nataf and Ricard, 1996) along the path. The source excitation is computed for a point double-couple using source parameters taken from the Harvard CMT catalog and the source region velocity structure of the 3D 3SMAC model.

To improve the reliability of the tomographic model, as well as to save computational time in the tomographic part of the analysis, the number of paths are reduced by using ‘summary rays’. Average models from neighbouring paths, which are defined as paths having end-points lying in the same areas of $A^\circ \times A^\circ$ are calculated. The value of $A=3^\circ$, which is smaller than the tomographic smoothing used in the next step of the procedure, was chosen. During this procedure, the root-mean-square deviation, σ_c , of the shear-velocity models in each group of paths is calculated. When σ_c exceeds a maximum threshold (0.1 km s^{-1}), the ‘outlier-models’ are searched for and discarded. Examples of raypaths and velocity models from two such groups of paths are shown in Fig. 2. This path-grouping procedure has reduced the dataset from about 9000 single paths to about 4700 grouped paths.

These group-averaged velocity models are then combined in a tomographic inversion using a continuous formulation of the inverse problem (Montagner, 1986) to obtain the local S_v -wave speed and azimuthal anisotropy at each depth. Lévêque et al. (1998) describe how the azimuthal anisotropy can be extracted in addition to the lateral variations in shear

wave velocity from the 1D path-average shear wave velocity model obtained from the Cara and Lévêque (1987) technique. The lateral smoothing in the tomographic inversion is controlled using a Gaussian a priori covariance function with scale length L_{corr} and standard deviation σ . L_{corr} defines the distance to which adjacent points of the model are correlated and acts as a spatial filter; σ controls the amplitude of the perturbation in Earth structure allowed (velocity perturbation, azimuthal anisotropy or both) in the inversion. The continuous regionalization approach used for the surface wave inversion provides an a posteriori error estimate for the extracted model, which is a useful guide to the resolution attainable from the data.

The main two underlying assumptions in the surface waveform tomography are: (1) the great-circle propagation and (2) the independent propagation of surface-wave modes. Pilidou et al. (2004) discuss the validity of these assumptions in more detail. Previous studies (e.g., Kennett, 1995; Yoshizawa and Kennett, 2002) have shown that the great-circle approximation is valid for surface waves crossing major structural boundaries, such as continent–ocean transitions, for periods longer than 50 s and path-lengths shorter than 10,000 km. The analysis is therefore restricted to relatively short paths and long periods. To avoid artifacts in the model from neglecting mode coupling (Marquering et al., 1996), the analysis is restricted to the fundamental and first four higher Rayleigh modes in the 50–160-s period band. This choice of modes and frequency range enables us to resolve the Earth structure between about 50 and 400 km depth (Debayle et al., 2001). The crustal structure is therefore fixed to that of the 3SMAC model and only for the 1D upper mantle structure along the path is inverted for.

3. Data

The North Atlantic is well placed with respect to global seismicity for surface wave tomography studies. Large earthquakes occur over a wide range of azimuths at near teleseismic distance and moderate earthquakes occur along the mid-Atlantic Ridge. A dataset of over 50,000 vertical-component Rayleigh wave seismograms with propagation paths crossing

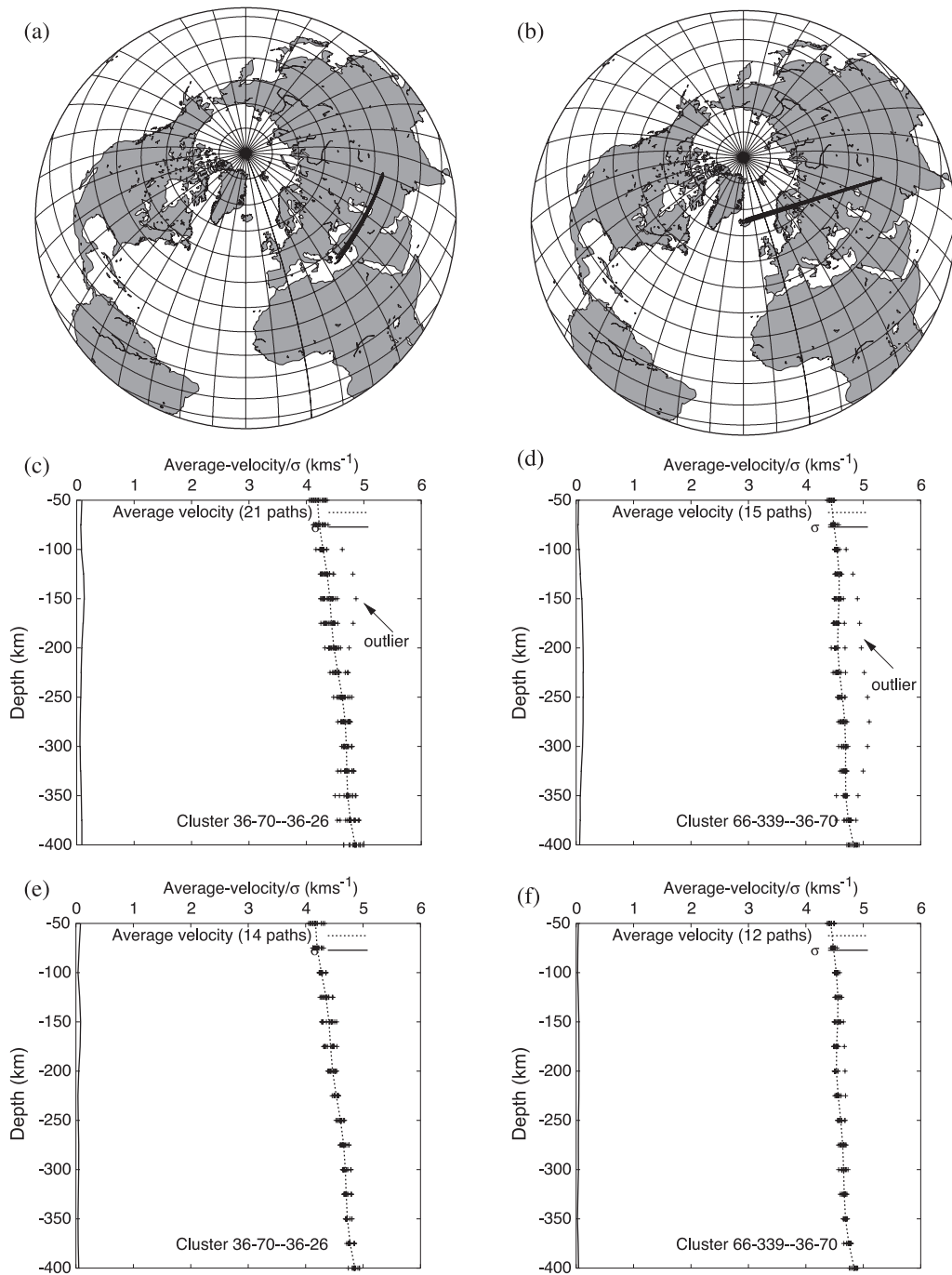


Fig. 2. Path-grouping examples from two groups of paths shown in (a) and (b), using $A=5^\circ$ (see text for details). In plots (c)–(f), the points represent all 1D shear velocity models of each cluster, the average velocity model is shown by the dotted line and the root-mean-square deviation of the models in shown by the solid line. (c) and (d) show all models, and (e) and (f) show the models finally considered for each cluster, after removing the ‘outlier-paths’.

the North Atlantic was assembled. These came from 1796 events occurring in the period 1977–2002 and recorded at 301 seismographs surrounding the North Atlantic (Fig. 3). About 92% of these seismographs come from IRIS, GEOSCOPE and GEOFON stations; additional seismographs come from national seismic networks in Canada, the USA, the United Kingdom, Denmark (including stations in Greenland), Norway, Sweden and Iceland, temporary seismographs of the IRIS, PASSCAL and ICEMELT deployments in Iceland, and the Danish GLATIS deployments in Greenland.

To improve the path coverage, additional stations were installed in Iceland, along the east coast of Greenland, the Faeroe Islands, Ireland, Scotland and Norway (Fig. 3) during 2000–2002 in places where there were gaps in the permanent station coverage.

Each site had a Guralp CMG3T sensor flat in velocity in the range 0.008–50 Hz but the data were recorded on various data loggers. The stations in Norway were incorporated into the Norwegian national seismic network and stations in Iceland into the SIL network. Stations in the Faeroe Islands, Ireland and Scotland were locally recorded on Reftek or Guralp SAM data loggers. All stations recorded data continuously at a rate of 100 samples per second and had GPS time.

The conservative waveform fitting procedure resulted in 8936 1D path-averaged velocity models from which the 3D velocity and azimuthal anisotropy Earth models are constructed. The path density (Fig. 4a) is greater than 200 paths per $4^\circ \times 4^\circ$ square over a broad region around Iceland and Europe; the azimuthal distribution of paths is good, especially in the eastern North Atlantic and west central Europe

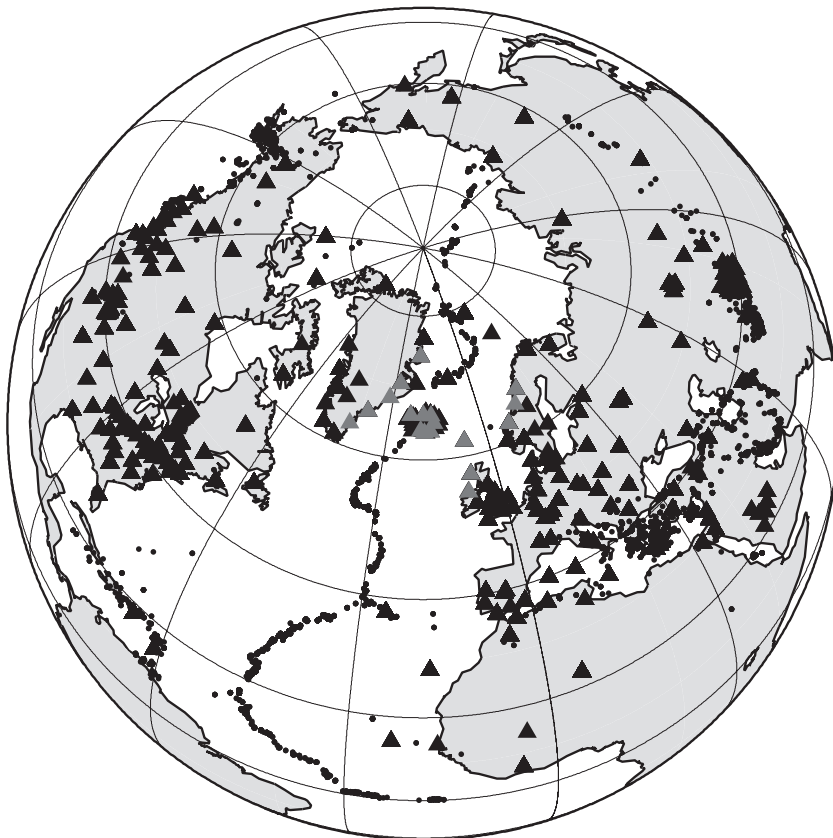


Fig. 3. Station and earthquake locations. Gray triangles denote the stations installed for this project, and black triangles denote stations from the IRIS, GEOSCOPE, GEOFON networks and stations from national seismic networks in Canada, the USA, the United Kingdom, Denmark (including stations in Greenland), Norway, Sweden and Iceland, as well as temporary seismographs of the IRIS, PASSCAL and ICEMELT deployments in Iceland, and the Danish GLATIS deployments in Greenland. Black solid circles denote the earthquakes' epicentres.

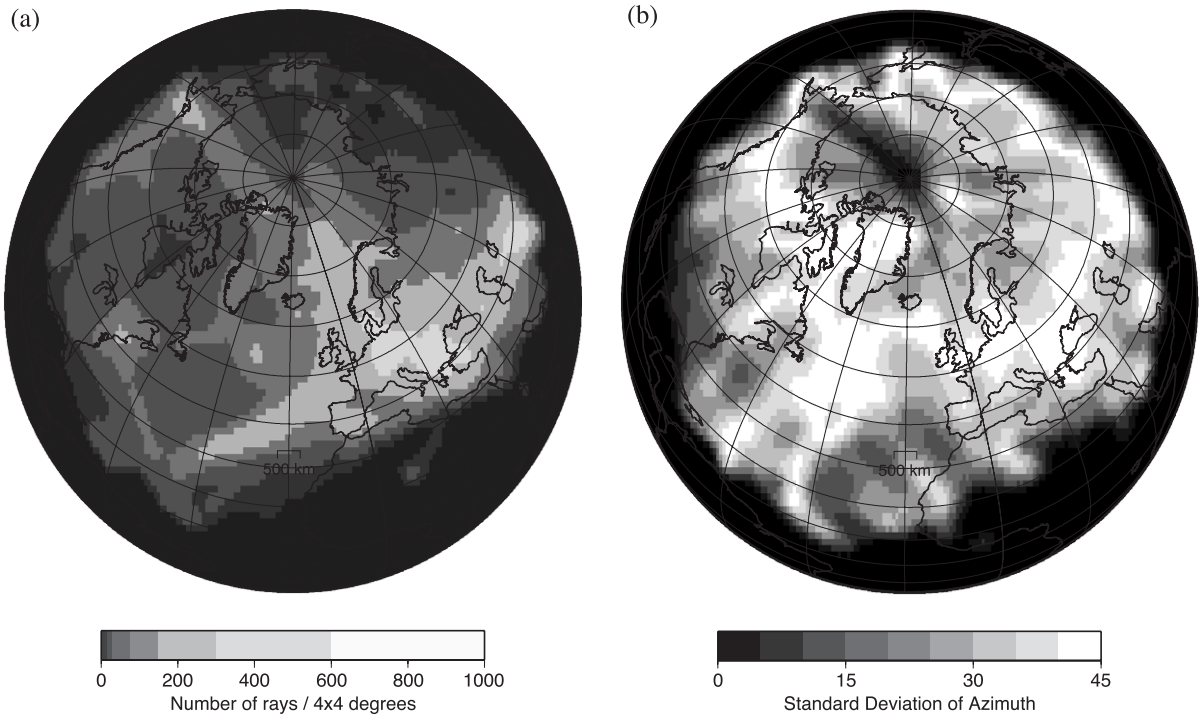


Fig. 4. (a) Ray density expressed as number of rays crossing $4 \times 4^\circ$ cells and (b) corresponding standard deviation of azimuths.

(Fig. 4b). The higher-mode coverage is not uniform; for example, western Europe has denser higher-mode coverage than the central North Atlantic Ocean because of the numerous deep earthquakes in the Aegean and eastern Mediterranean.

Shown in Fig. 5 are five examples of typical waveform fits for a variety of epicentral distances and source depths. Good waveform fit is achieved for both higher modes (clearly seen in (a) and (b)), and the fundamental mode, despite the considerable misfit between the observed seismograms and initial synthetic-seismograms.

4. Heterogeneity and azimuthal anisotropy beneath the North Atlantic

The S_V -wave velocity heterogeneity and azimuthal anisotropy model for the North Atlantic is shown in Figs. 6 and 7. The background color scale represents the variation in seismic wave speed and the bars represent the local direction of fast horizontal propagation of S_V -waves. The length of the bars is

proportional to the peak-to-peak azimuthal anisotropy. If the upper mantle anisotropy primarily results from the preferred alignment of olivine crystals, the direction of fast S_V -wave propagation is expected to be along the projection of the fast α -axes of olivine in the horizontal plane (Lévêque et al., 1998).

The model shown in Fig. 6 was obtained using $L_{\text{corr}}=400$ km for both velocity heterogeneity and azimuthal anisotropy, $\sigma=0.05$ km s^{-1} for the velocity perturbation and $\sigma=0.003$ km s^{-1} for the azimuthal anisotropy variation. This choice favors a smooth model considering the shortest wavelengths (about 200 km at 50-s period) and the dense path coverage.

The a posteriori error maps (Figs. 8 and 9) display a pattern very similar to that of the path distribution (Fig. 4a). The gray areas in Fig. 6 denote regions with an a posteriori error greater than 0.04 km s^{-1} and correspond to regions of poor resolution, i.e., regions where the a posteriori error is close to the a priori error (0.05 km s^{-1}). The resolution is best where the a posteriori error is small. These error maps show that the resolution is significantly better in central Europe, especially at depth, than in the central Atlantic Ocean.

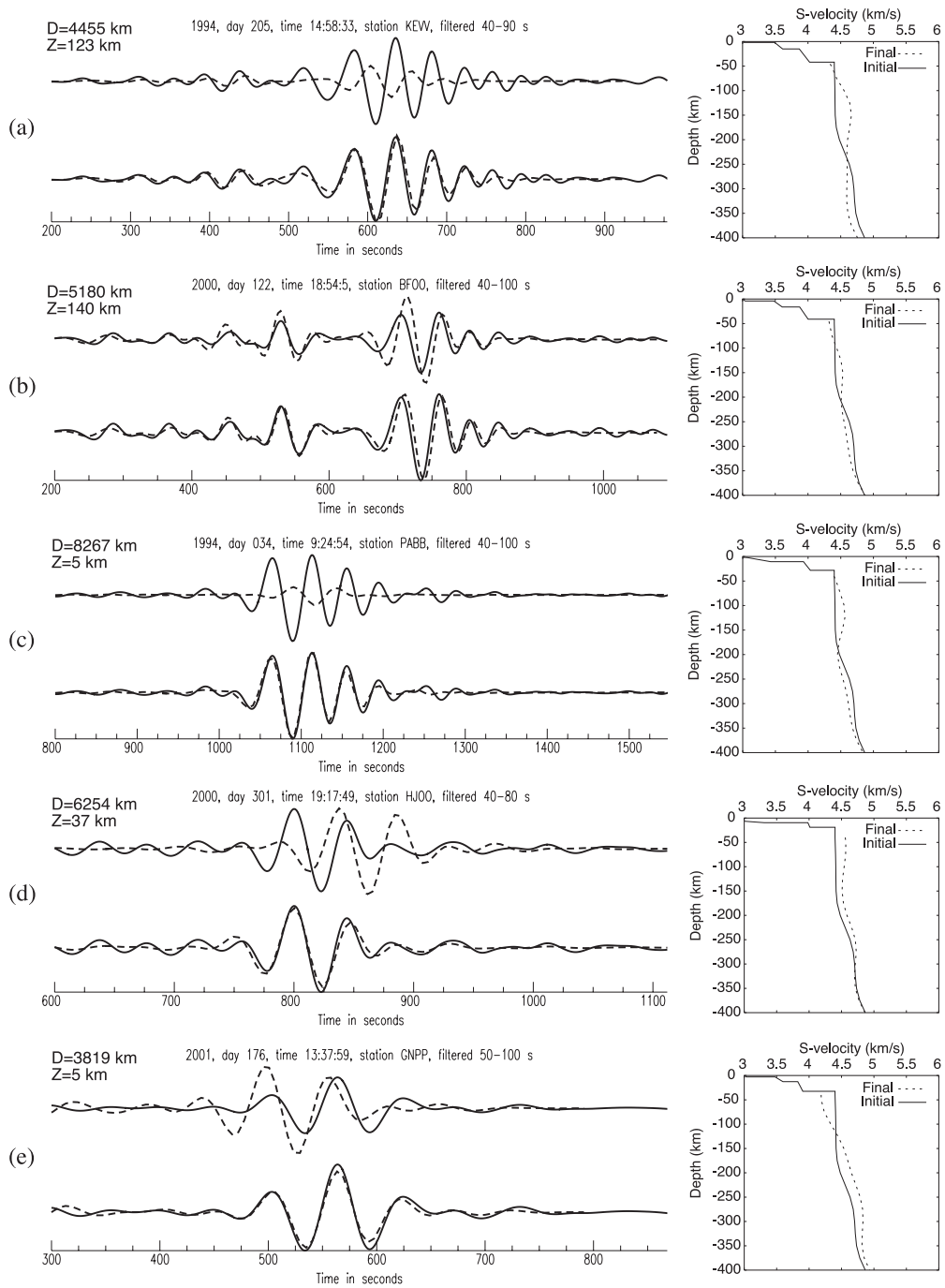


Fig. 5. Examples of waveform fits and the resulting 1D path-averaged S_v -models before and after the 1D inversions for five different paths. Synthetic waveforms are denoted by dashed lines and observed waveforms by solid lines. In each case, the top and bottom traces are the initial and final fits, respectively, and at the right the solid and dashed lines denote the initial and final S_v -models, respectively. The epicentral distance, D , and focal depth, Z , are shown at the top left corner of each plot. Waveforms (a), (b) and (c) were recorded by permanent IRIS stations, whereas waveforms (d) and (e) were recorded by stations deployed by us in Greenland and Ireland, respectively.

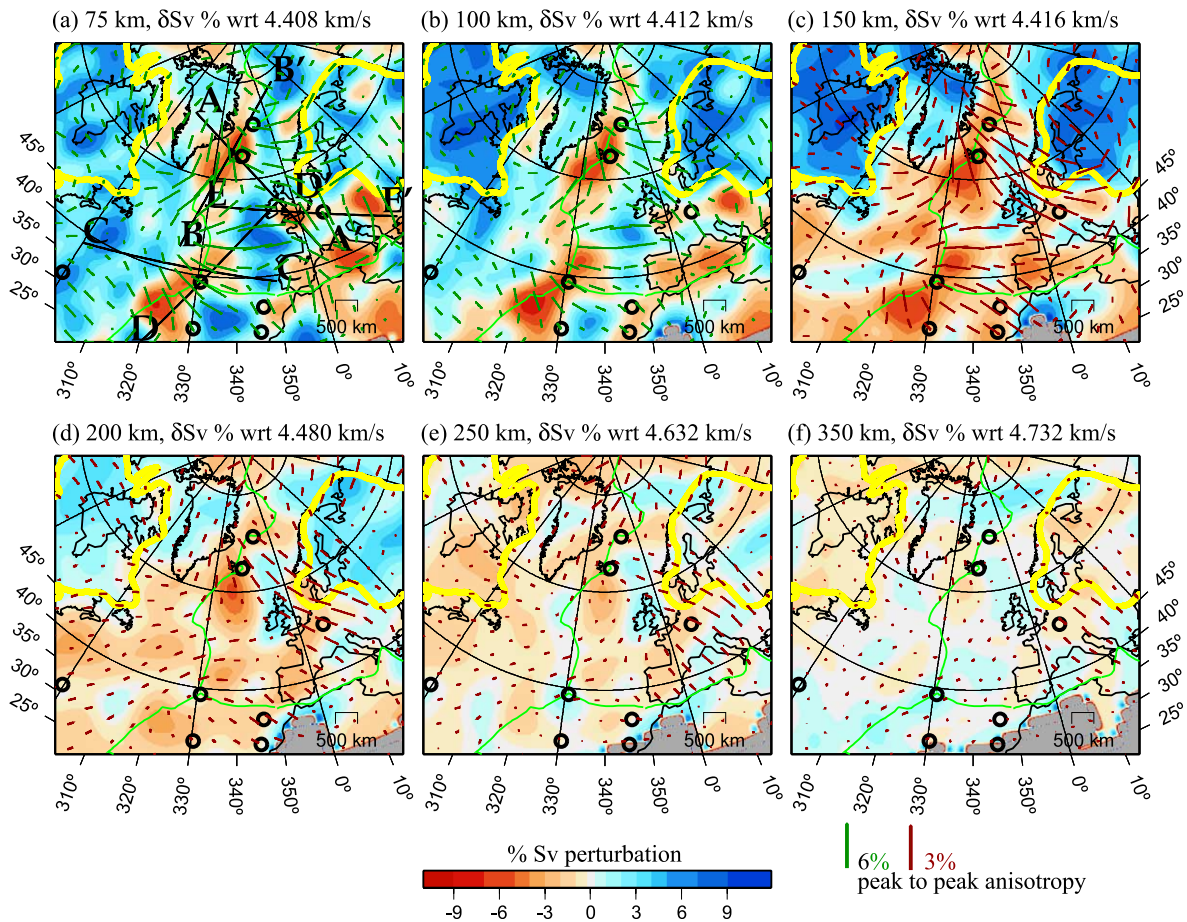


Fig. 6. S_v -wave heterogeneity and azimuthal anisotropy distribution at depths of (a) 75, (b) 100, (c) 150, (d) 200, (e) 250 and (f) 350 km. The heterogeneity is shown as the departure from a smooth PREM mantle model. Red and blue colours represent areas of slower and faster velocities, respectively, with respect to the reference model. The fast directions of horizontally propagating S_v -waves are shown by the light-green (a–b) or red (c–f) bars, the length of which is proportional to the peak-to-peak azimuthal anisotropy. Gray areas denote regions with an a posteriori error (Fig. 8) greater than 0.04 km s^{-1} and correspond to regions of poor resolution. In all plots, the solid green line defines the plate boundaries and the solid yellow lines refine the Canadian and East-European craton boundaries. The depths and reference velocities are indicated at the top of the plots. The vertical cross-sections along the 4300-km long profiles AA' to EE', marked on map (a), are shown in Fig. 7.

The good depth resolution in central Europe is clear from profile EE' (Fig. 9).

The main features of the results are similar to those of our previous model (Pilidou et al., 2004), which was derived from 3000 paths, only a third of the number of paths used in this study. The main features of our new model derived from the analysis of the 9000 paths do not differ from those of the earlier model derived from analysis of the 3000; however, the resolution has improved (compare Fig. 6(a) with Fig. 12) and some of the fine details have changed.

A high degree of S_v -wave speed heterogeneity ($\pm 8\%$) and a large-amplitude (up to 3%), complex azimuthal anisotropy pattern characterize the shallow (75–150 km depth) layers. Both the amplitude of the S_v -wave speed heterogeneity and the complexity and amplitude of the azimuthal anisotropy decrease with depth. In the deeper parts of the model (>200 km depth), the S_v -wave speed heterogeneity is reduced to $\pm 2.5\%$ and the amplitude of the azimuthal anisotropy to 1%.

There are a number of well-known features in the mantle model. High velocity roots exist beneath the Canadian and Greenland shields in North America

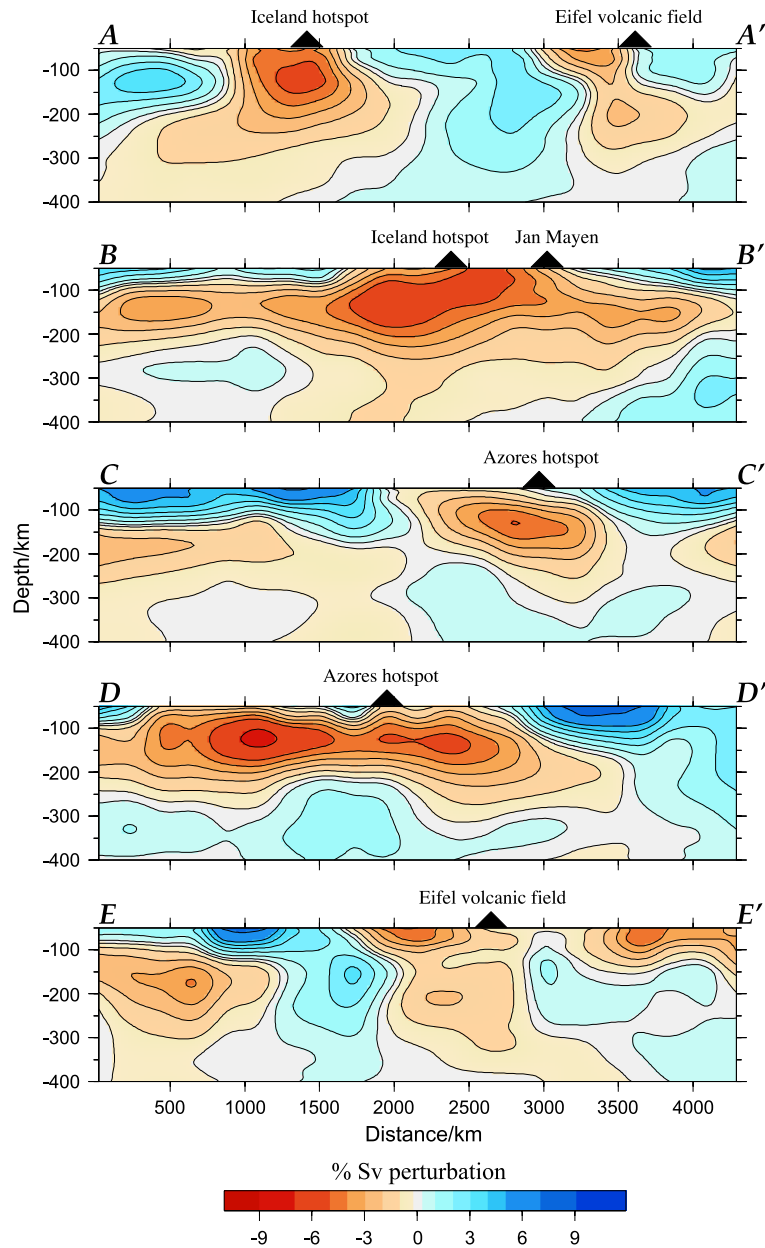


Fig. 7. Vertical cross-sections along the 4300-km long profiles AA' to EE', marked on Fig. 6(a). The heterogeneity is shown as percentage departure from the smoothed mantle PREM model.

and beneath the Baltic shield and the East European Platform in Europe (Fig. 1). All these high velocity roots are very well resolved and persist to approximately 225 km depth. At 150 km depth, there is a well-defined boundary between the high velocities observed beneath the East European Platform and low

velocities observed beneath the tectonically younger parts of central Europe, coinciding with the Tornquist-Teisseyre zone (TTZ) as previously noted in the studies of Zielhuis and Nolet (1994), Marquering and Snieder (1996) and Marquering et al. (1996). There is a clear thickening of the oceanic lithosphere with

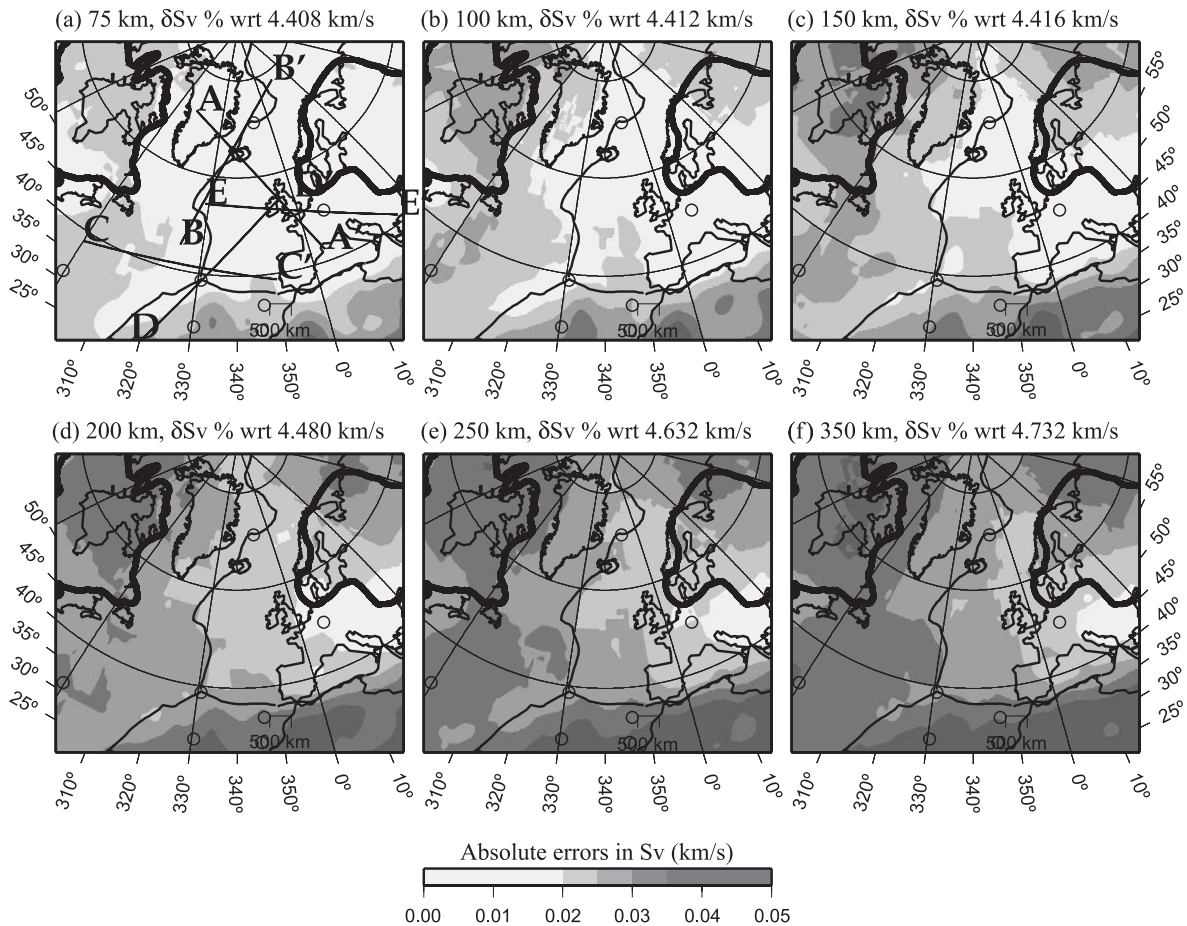


Fig. 8. A posterior absolute error distribution of S_v for the sections shown in Fig. 6. The a priori error was set to 0.05 km s^{-1} . The depth is indicated at the top of each plot. The vertical sections along the profiles marked on map (a) are shown in Fig. 9.

increasing distance from the mid-Ocean ridge (Zhang and Lay, 1999). At 100 km depth, low upper mantle velocities exist beneath the Tyrrhenian Basin (Faccenna et al., 2003).

Low-velocity anomalies occur in the upper mantle beneath three major hotspots: Eifel, Iceland and the Azores. The Eifel hotspot is located in NW Europe, a slow moving plate. This area of the model has the best depth resolution (Fig. 9, profile EE). The low-velocity anomaly beneath the Eifel hotspot is much weaker than that previously observed (Pilidou et al., 2004), but it still extends to the bottom of the model at 400 km depth. Iceland is located on the mid-Atlantic Ridge and the Azores are located near the ridge. The upper mantle low-velocity anomalies beneath both of these hotspots are elongated along the direction of the

ridge and extend to about 200 km depth. There is no evidence of a slow anomaly extending deeper than 200 km. The low-velocity structures associated with these three hotspots are discussed in more detail in Section 6. The model reliability and resolution was investigated through several synthetic-seismogram experiments and other tests, which are discussed in the following section.

5. Reliability and resolution of the 3D model

There are a number of factors which could introduce artifacts and bias into the tomography model. These include errors in the theory and approximations such as assuming great-circle prop-

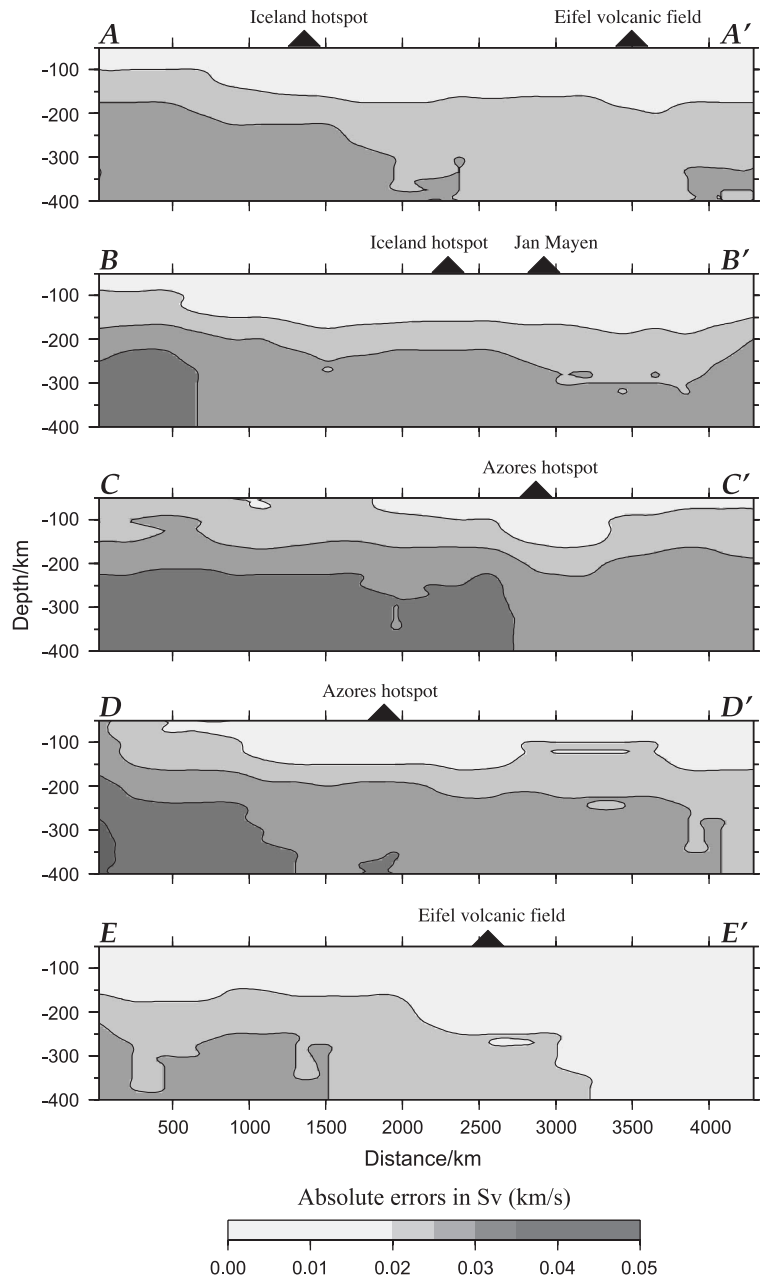


Fig. 9. Vertical cross-sections through the a posteriori error model along the 4300-km long profiles AA' to EE', marked on Fig. 8(a).

agation, neglecting mode coupling, using an inappropriate starting model for the waveform inversions and poor knowledge of the non-inverted parameters such as the earthquake hypocentral coordinates and focal mechanism and the fixed crustal model. As discussed above, errors in the tomographic model resulting from

the great-circle approximation are minimized by choosing relatively short propagation paths and artifacts in the tomographic model resulting from ignoring mode coupling are minimized by considering only the fundamental and first four higher modes for periods greater than 50 s.

Cara and L ev eque (1987) show that for their waveform inversion technique, the final velocity structure is weakly dependent on the reference and inversion starting model. Errors in the source parameters will cause errors in the 1D path-average velocity models, but there is no reason for these effects to be coherent since they relate to earthquakes with different source mechanisms covering a wide area; the errors are expected to average out in the tomographic inversion if, as in this study, a large number of paths with different azimuths are used to constrain the structure.

An extensive series of experiments performed using a subset of this dataset, but covering the same area of the North Atlantic is described by Pilidou et al.

(2004). The results from two of their synthetic-seismogram resolution experiments are shown in Figs. 10 and 11. In this section, the conclusions from these tests are briefly discussed. However, the limiting resolution implied by these tests is the minimum resolution expected for the current model, which encompasses 300% more data.

As discussed above, the crustal structure is kept fixed to the path-specific structure, calculated from the 3SMAC model (Nataf and Ricard, 1996), while inverting for the mantle structure. This is necessary because surface waves are sensitive to the crustal structure even though their wavelengths are too long to constrain it. Therefore, poor constrains on the fixed

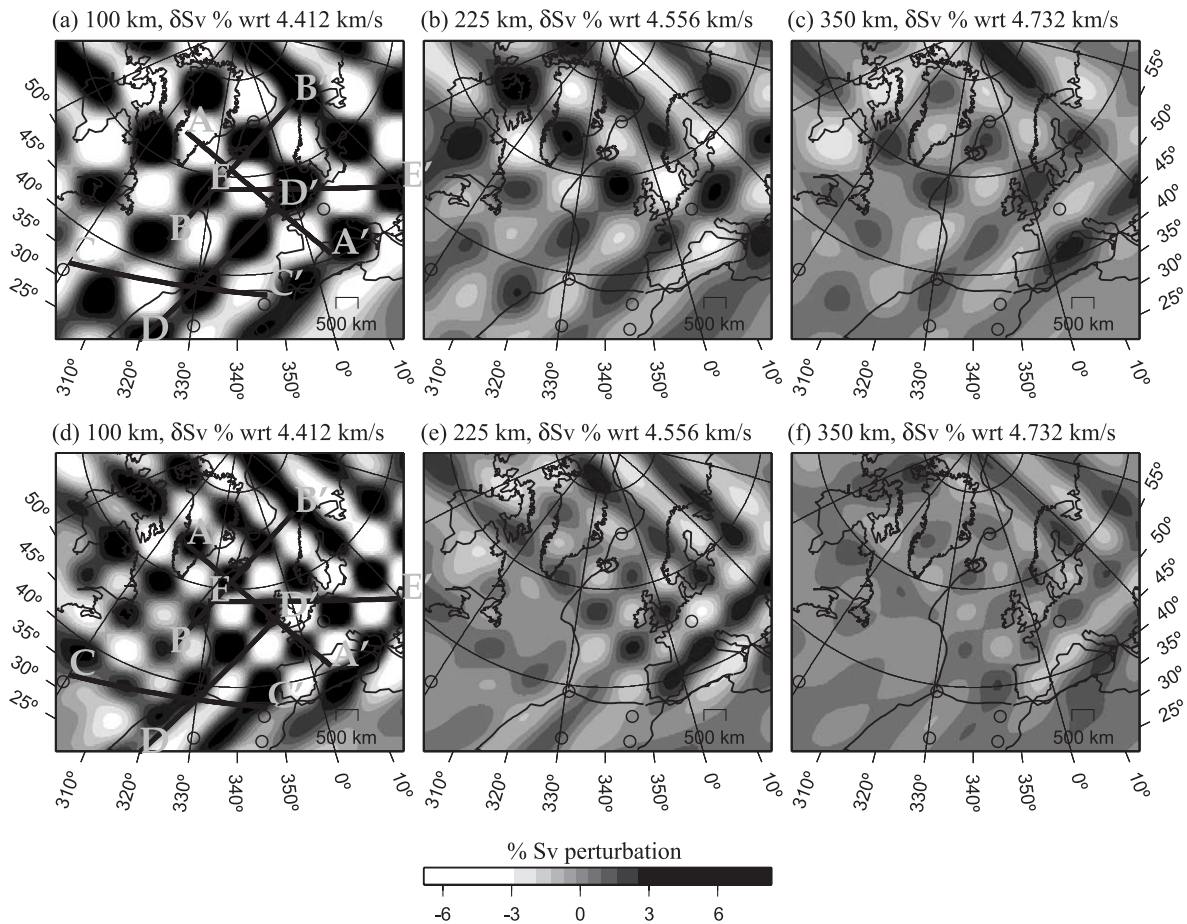


Fig. 10. Recovered models from two synthetic-seismogram experiments of Pilidou et al. (2004), using a subset of the dataset presented in this study. The input model is a 3D ‘checkerboard’ structure, with 3D blocks of alternating speed heterogeneity of $\pm 6\%$, vertical extends of 100 km and horizontal extends of $10^\circ \times 10^\circ$ (a–c) and $7^\circ \times 7^\circ$ (d–f). The vertical sections through the models along the profiles marked on maps (a) and (d) are shown in Fig. 11.

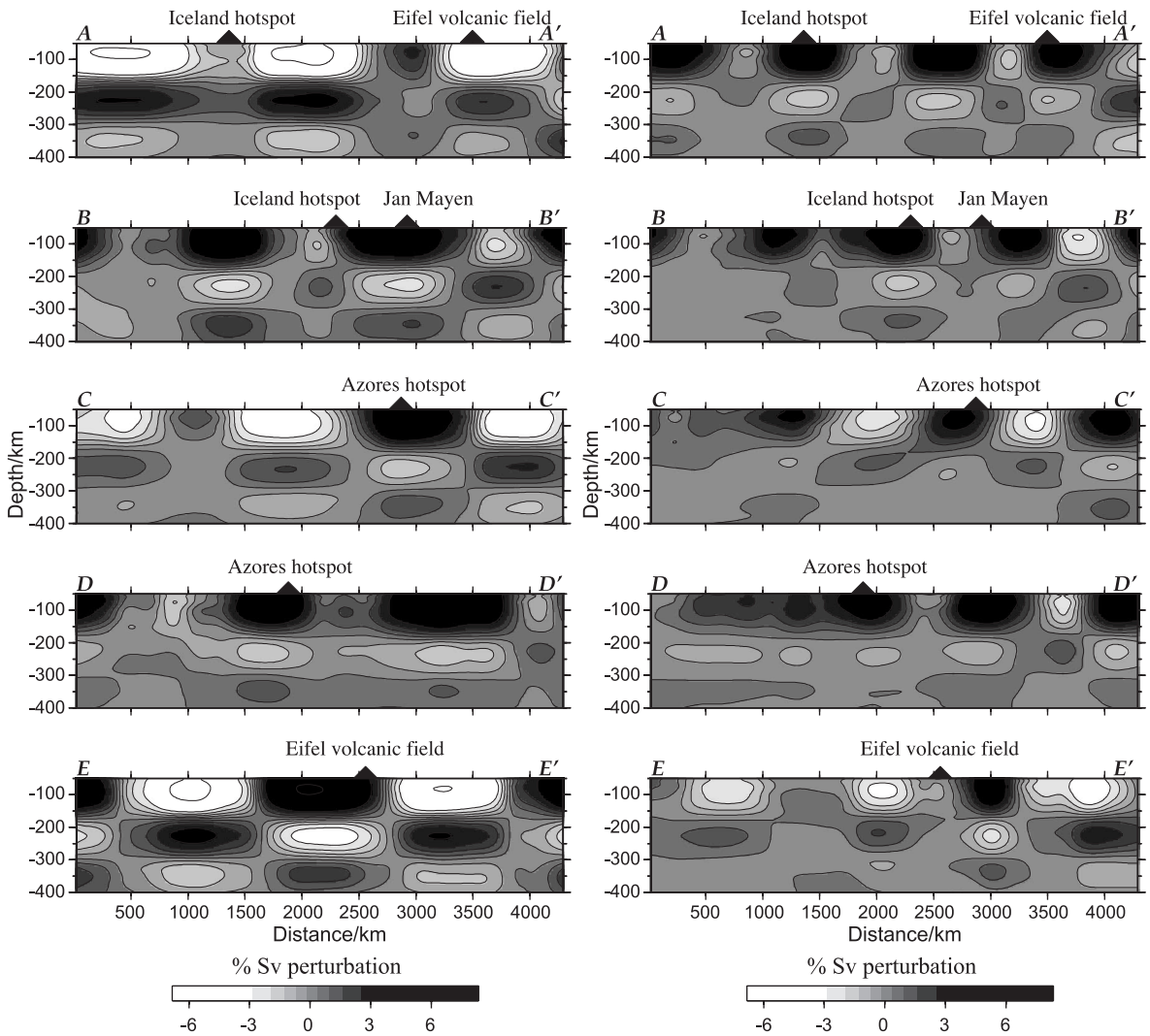


Fig. 11. Recovered models from two synthetic-seismogram experiments of Pilidou et al. (2004). Vertical cross-sections along the 4300-km long profiles AA'–EE', marked on Fig. 10(a),(d).

crustal structure can bias the mantle structure. To assess the validity of the choice of the 3SMAC model, Pilidou et al. (2004) re-inverted the complete waveform dataset using an updated version of CRUST2.0 (Bassin et al., 2000) for the crustal model. The results showed that most differences between the two inversion results occur at depths shallower than 100 km, where the images obtained using CRUST2.0 are less complex and have a stronger resemblance to the surface tectonics than the image obtained using 3SMAC. However, the choice of the crustal model has little effect on the deeper parts of the model.

Pilidou et al. (2004) performed a number of synthetic-seismogram experiments to test the resolution of the S_V -wave speed heterogeneity attained in the model. The resolution is controlled by the density and azimuthal distribution of the paths and the frequency content and modal-composition of the surface waves. In each test, multi-mode synthetic seismograms are calculated for propagation paths through a simple 3D input model for the same source parameters and event-receiver combinations as in the actual data. The synthetic surface waveforms are analyzed in exactly the same way as the actual data

using the automated analysis procedure outlined in Section 2. Since the synthetic seismograms are inverted for the same frequency content and mode combinations as in the real data, these tests not only provide information on the spatial resolution of the model from the path coverage, but since the 1D inversion step is repeated, the tests also provide information on the depth resolution.

Such experiments (see Figs. 10 and 11), using “checkerboard” input models consisting of alternating slow and fast blocks of variable extents, showed that the geometry of the input model is generally well recovered, both laterally and vertically everywhere in the model, whereas the amplitude recovery is best in the top 150 km and falls off with depth. The deep structure is most faithfully recovered along profile EE’ (see Fig. 7) because of the dense higher-mode coverage in western Europe.

Pilidou et al. (2004) also performed synthetic-seismogram experiments designed to determine whether the amplitude decay with depth of the low-velocity anomaly associated with the Iceland Plume (sections AA’ and BB’ of Fig. 6) is real, or an artifact due to the specific frequency and higher-mode content of the dataset. These tests have shown that the low-velocity feature beneath Iceland seen in the model does not extend to a depth greater than 200 km, because such a broad structure would have been resolved by the long-period and higher-mode dataset. The authors also investigated the possibility of resolving a narrow (200 km wide), plume-tail structure beneath Iceland, by a series of experiments using a ‘plume-like’ structure as a starting model, and repeating the tomographic inversions with different values of L_{corr} . The results showed that the presence of the plume stem is detected, but its exact shape and amplitude are not properly resolved, suggesting that the fact that a narrow, low-velocity feature is not observed below 200 km in the upper mantle does not rule out the existence of a plume tail at those depths.

Pilidou et al. (2004) finally performed a series of synthetic-seismogram experiments to both test the resolution of azimuthal anisotropy and the magnitude of the trade-off between heterogeneity and azimuthal anisotropy. The results suggested that the anisotropic pattern obtained with surface waves can be locally wrong in regions where changes in anisotropic

direction would occur over distances much smaller than a wavelength. For this reason, only the general trend of the anisotropy will be discussed in the next section. These tests also show that 5% peak-to-peak anisotropy can result in 2% heterogeneity, whereas 6% heterogeneity can result in 0.7% peak-to-peak anisotropy. This places bounds on the magnitude of the azimuthal anisotropy that can be interpreted in the model.

A checkerboard tomography test is performed with the current dataset. In this test, 1D path-averaged models are calculated for each one of the 9000 paths crossing a 3D checkerboard model consisting of a regular pattern of alternating velocity perturbations, $\pm 6\%$ slow with respect to PREM. These paths are then grouped together and group-averaged models are calculated in exactly the same way as with the actual data, described in Section 2. The tomographic step of the procedure is finally repeated, using the a priori errors of the 1D models resulting from the waveform inversions of the actual data. This test only provides information on the horizontal resolution. The result, shown in Fig. 12, shows that the larger dataset gives excellent lateral resolution in all parts of the model.

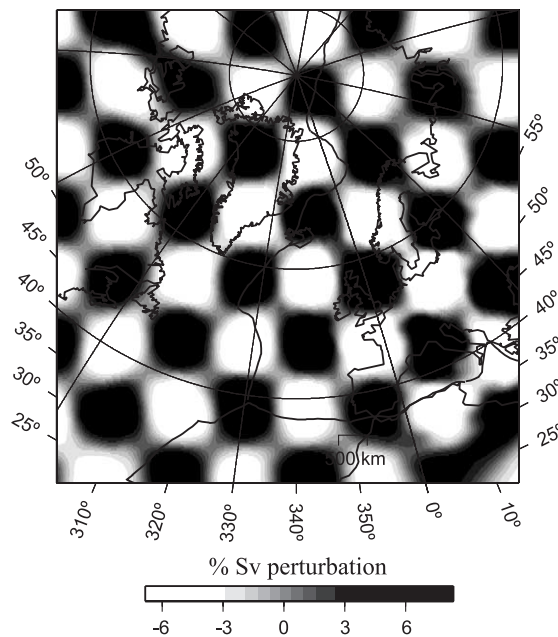


Fig. 12. Recovered model from a tomographic inversion experiment for the dataset used to build the tomographic model shown in Figs. 6 and 7.

6. Discussion

6.1. Shear-velocity heterogeneity

The tests performed with a subset of the data show the tomographic model for the North Atlantic and surrounding region to be reliable and robust. The upper mantle structure at depths greater than 100 km depth is not likely to contain significant artifacts resulting from the choice of a fixed crustal model. The synthetic-seismogram tests suggest that input heterogeneities with wavelength of at least 700–1000 km should be well recovered both laterally and vertically throughout the model down to 400 km depth. The amplitude of the anomalies is well recovered in the upper 150 km of the model, but the amplitude of features is increasingly underestimated with increasing depth. Azimuthal anisotropy is well resolved in the areas of good azimuthal path coverage, including the area around Iceland. Synthetic-seismogram experiments show that the trade-off between heterogeneity and anisotropy does not exceed 2%.

6.1.1. The Iceland Plume

The Iceland Plume has a high heat flux (Sleep, 1990) and is centered beneath a slow spreading ridge. The upper mantle low-velocity anomaly associated with Iceland is of varying diameter and extends to a depth of about 200 km (Fig. 7, profiles AA' and BB'), but has a somewhat smaller lateral extent than the anomaly imaged with a smaller dataset (Pilidou et al., 2004). At 75–125 km depth, the low-velocity anomaly is 4–7% slower than PREM, centred on Iceland and elongated along the direction of the mid-Atlantic Ridge with dimensions of about 1,700 km along the ridge and 600 km perpendicular to the ridge. At 150 km depth, the anomaly is strongest in the southwest of Iceland where it is approximately circular with a diameter of about 1000 km. Between 175 and 350 km depth, the low-velocity anomaly decays to the PREM background level. Between about 100 and 200 km depth, the low-velocity anomaly in the SW of Iceland has an almost constant S_v -velocity of $(4.10 \pm 0.05) \text{ km s}^{-1}$. Priestley and Tilmann (1999) found the same velocity in this depth range beneath Hawaii, another high heat flux plume (Sleep, 1990) and attributed these low velocities to plume material

ponding beneath the plate. The low velocity observed beneath Iceland is averaged over a distance of 800 km centered on Iceland (Fig. 7, profile AA'). The observed velocities at these depths are slightly lower than the shear wave velocity thought to occur in the asthenosphere beneath 0–20 Ma oceanic lithosphere (Nishimura and Forsyth, 1989) for a fast-spreading ridge. Similar low shear wave velocities were found by Allen et al. (2002b) between the Moho and 200 km depth in a more restricted region beneath Iceland.

The low-velocity anomaly observed in the North Atlantic beneath Iceland has a significantly larger NS dimension along the ridge axis than the EW dimension perpendicular to the ridge axis. In the south, it extends for about 1200 km along the Reykjanes Ridge. Numerous observations indicate that the Reykjanes Ridge segment of the mid-Atlantic Ridge south of Iceland is modified by the plume. For more than 1000 km to the south of Iceland, the sea floor is anomalously shallow (Vogt, 1971), the topography is much smoother and lacks segmentation and an axial valley typical of slow-spreading ridges (Searle et al., 1998), and the crust is anomalously thick (Smallwood and White, 1998). Gravity and bathymetry data show prominent V-shaped anomalies (Vogt, 1971) along the ridge which correlate with local variations in crustal thickness. Isotope and trace element ratios measured along the Reykjanes Ridge are different from those measured along ridge segments located away from active plumes and indicate a mixing of an enriched plume source and Mid-Ocean Ridge basalt (MORB) source (Schilling, 1973; Fitton et al., 1997). All these observations are indicative of plume material flowing laterally along the ridge, from the plume centered beneath Iceland. Gaherty (2001) finds that Rayleigh waves propagating south of Iceland along paths parallel to the Reykjanes Ridge arrive at the predicted time but Love waves arrive late, indicating anisotropy but of the opposite sign to that normally observed for Rayleigh and Love waves. He attributes this unusual form of anisotropy to the supply of heat beneath the ridge, which drives a sheet-like mantle upflow beneath the ridge to a depth of about 100 km. The V-shaped gravity, bathymetry and crustal thickness variations along the ridge are thought to reflect a time-variation of the Iceland Plume (Vogt, 1971).

The low-velocity anomaly extends for about 600 km in the north of Iceland, along the Kolbeinsey Ridge (Fig. 1). Various observations indicate the existence of plume material underlying the ridge in this area. The Kolbeinsey Ridge is unusually elevated between the Tjörnes fracture zone, immediately in the north of Iceland, and Jan Mayen, about 1000 km further north. A plume is believed to exist under Jan Mayen (Schilling, 1985). Jones et al. (2002) show that gravitational V-shaped ridges are visible between the Spar Fracture zone (located about midway between Iceland and Jan Mayen, at approximately 500 km north of Iceland) and Jan Mayen. These are only apparent to the east of the ridge, probably because thick sediments from Greenland cover much of area west of the ridge. Schilling et al. (1999) found that the boundary on the Kolbeinsey Ridge between the zone of influence of the “low $^3\text{He}/^4\text{He}$ ” Jan Mayen Plume and the “high $^3\text{He}/^4\text{He}$ ” Iceland Plume is in the vicinity of the Spar Fracture zone. Taylor et al. (1993) show that the Sr, Nb and Pb isotope signature of the Iceland Plume is as widespread as the thermal and topographic anomalies around Iceland and that the Kolbeinsey Ridge is significantly affected by the Iceland Plume but less so than the Reykjanes Ridge to the south of Iceland. The low-velocity anomaly north of Iceland could therefore result from either of two causes: The influence of the Iceland Plume for about 500 km in the north along the Kolbeinsey Ridge, or a plume under Jan Mayen.

Alber and Christensen (2001) investigate the interaction of a mantle plume with a mid-Ocean Ridge in a 3D numerical modelling experiment, using a strongly temperature-dependent viscosity model, to determine how the shape and size of a plume head depends on the various model parameters. They find that for a strong, plume-like structure beneath a slow-spreading ridge, the plume material rises to the base of the plate and spreads laterally but preferentially along the ridge axis. The thickening lithospheric plate perpendicular to the ridge forms an upper boundary of an elongated wedge-shaped region which confines the material in the plume head, causing most of the plume material to flow along the ridge until it cools and becomes part of the newly generated lithosphere. For a model plume with the parameters appropriate for the Iceland Plume, Alber and Christensen (2001) find the along-axis plume dimension is 1800 km and

the aspect ratio (ratio of along-ridge to across-ridge length) of 3.16. At 100 km, the low-velocity feature centered beneath Iceland has a total length of about 1700 km and width of about 600 km, resulting in an aspect ratio of 2.8.

Between 175 and 350 km depth, the low-velocity anomaly beneath Iceland decays to the PREM background level. This decay is stronger than the apparent reduction in the anomaly amplitude with depth due to the frequency content and modal composition of the surface wave data (Pilidou et al., 2004). This image of the low-velocity anomaly in the upper mantle beneath Iceland is of higher lateral resolution, but compatible with the models of Ritsema et al. (1999) and Zhao (2001) at shallow (<175 km) depths. A narrow plume stem is not resolved at deeper depths beneath Iceland as is in the model of Ritsema and Allen (2003). However, this could be a result of insufficient higher-mode coverage, as discussed below. Allen et al. (1999) investigate diffraction effects of a cylindrical plume stem on the frequency dependence of shear wave arrivals measured on Iceland and conclude the plume stem must have a radius of about 100 km and a maximum S-velocity anomaly of -12% . Allen et al. (2002a) conclude from the analysis of a variety of seismic data that, from 250 to 400 km beneath Iceland, there exists a near-cylindrical low-velocity anomaly with a radius of 100 km and a peak S-velocity anomaly of -4% . Our tests (Pilidou et al., 2004) show that such a structure would only be resolved where the higher-mode content of the data is high, such as in central Europe (Fig. 9, profile EE'). A plume stem would not be resolved beneath the central North Atlantic Ocean (Fig. 9, profiles AA' and BB') considering the frequency content of the data (<0.02 Hz) and lateral smoothing (400 km) used in building the tomographic model.

6.1.2. The Azores Plume

The second major negative anomaly in the North Atlantic lies in an extended region beneath the Azores (Fig. 7, profiles CC' and DD'). This anomaly, like the one associated with Iceland, is elongated along the ridge axis. At 75–150 km depth, it extends between about 25°N and 45°N , a lateral extent significantly larger than that of the Iceland Plume (about 2200 km along-axis and 800 km perpendicular to the ridge). The Azores anomaly is both thinner vertically (75–

150 km depth) and decays more rapidly with depth than the Iceland Plume (compare profiles AA' with CC' and BB' with DD'). These differences are also present in the global tomography results of Ritsema et al. (1999) shown in Montagner and Ritsema (2001).

Even though the Azores hotspot is located 100 km east of the mid-Atlantic Ridge, long wavelength bathymetric, gravimetric and geochemical anomalies in this region indicate plume–ridge interaction. Rare earth element concentrations (Schilling, 1985) and Sr isotope ratios (Goslin et al., 1998; Dosso et al., 1993) indicate mixing of MORB and mantle plume source for 1800–1900 km along the ridge. But the mixing is not symmetric; the ridge is geochemically affected ~1200 km to the south but only ~600 km to the north (Goslin et al., 1998) of the Azores. Gravity and bathymetry show oblique V-shaped ridges in the south to 27° N (Thibaud et al., 1997). There are no V-shaped ridges to the north of the hotspot and the geochemical anomaly only extends to 43–44°N (Goslin and Triatnord Scientific Party, 1999).

Ito and Lin (1995) studied the variation of the bathymetry and gravity anomalies associated with five oceanic hotspots with comparable heat fluxes, including Iceland and the Azores, with the ridge-spreading rate and the hotspot–ridge axis separation. They found that the along-axis widths of the anomalies decrease with increasing spreading rate and increasing ridge–hotspot distance and that the temperature anomaly of the plume material at the ridge axis decreases with increasing ridge–hotspot distance. The ridge full-spreading-rates near Iceland and the Azores are 1.9 and 2.5 cm year⁻¹, respectively. Thus, Ito and Lin (1995) predict a weaker and smaller ridge anomaly for the Azores compared to Iceland, whereas similar anomalies are observed under both regions in the model presented here. Schilling (1991) also predicts a weaker temperature anomaly for the Azores in comparison to Iceland, implying a higher plume viscosity for the Azores Plume, or a smaller viscosity contrast between the plume and the surrounding mantle than for the Iceland Plume. The 3D numerical modelling experiments of Alber and Christensen (2001) show that when the viscosity contrast decreases, the plume head tends to be shallower, consistent with our observations, but becomes less elongated along the ridge axis, inconsistent with our tomographic results. However, the ridge spreads

obliquely in the Azores area, which could cause an increase of the along-axis width of the anomaly, resulting in a similar lateral extent of the Iceland and Azores plume heads.

6.1.3. *The Eifel Plume*

In the area of the Eifel hotspot (Fig. 1), the path density and azimuthal coverage are excellent (Fig. 4). Resolution tests (Pilidou et al., 2004), as well as the a posteriori error distribution (Fig. 9, profile EE'), show that this is in the best resolved region of the model.

The Eifel volcanic field located in the Rhenish Massif, NW Germany, is the result of the product of about 300 small volcanic eruptions which occurred between 700,000 and 10,800 years ago. Although the total volume is small (less than 15 km³), ongoing mantle helium outgassing (Griesshaber et al., 1992) and isotopic and trace element signatures (Hoernle et al., 1995) support a plume origin for these volcanics. Ritter et al. (2001) and Keyser et al. (2002) invert P- and S-wave travel times recorded on a large seismic network across the Eifel volcanic field and find a low-velocity zone about 100 km in diameter extending to at least 400 km depth. The S-wave velocity contrast is depth-dependent and varies from -5% at 31–100 km depth to at least -1% at 400 km depth.

The anomaly observed in this area in the current model is similar in extent, but much weaker in strength compared to our previous results (Pilidou et al., 2004). At 75 km depth, a low-velocity anomaly of approximate magnitude of -5% occurs beneath southeastern Great Britain. A strong negative anomaly occurs in the same geographical location at 80 km depth in the model of Marquering and Snieder (1996). With increasing depth, this low-velocity feature shifts to the east to approximately below the location of the Eifel hotspot. At depths greater than 100 km, the amplitude decreases to -2% and remains constant until 350 km depth, except for a thin zone between 150 and 250 km depth, where the magnitude increases to -3%.

6.2. *Azimuthal anisotropy*

The azimuthal anisotropy results obtained for the North Atlantic in the 75–300 km depth range are

shown in Fig. 6. The overall pattern is the same over these depths, but the amplitude of the azimuthal anisotropy decreases with depth. At 100–200 km depth, the amplitude of the azimuthal anisotropy is larger in the European plate than it is on the North American plate, but this difference also decreases with increasing depth. In the North Atlantic south of 50°N, the fast S_v -direction is perpendicular to the ridge axis but north of 50°N the pattern changes from having a EW fast axis to having a NS fast axis. There are three regions where there is a significant change in the azimuthal anisotropy pattern at 100 km depth: the region in the North Atlantic south of Iceland, NW Europe near the location of the Eifel Plume and near the low-velocity anomaly beneath the Iberian Peninsula.

Shear-wave splitting measurements at a number of stations across Iceland also give a consistent NW–SE fast polarization direction (Bjarnason et al., 1996, 2002; Li and Detrick, 2003), except in the area near the west coast, where the average direction is N–S. The anisotropy measurements resulting from body waves, which sample the structure directly beneath the Iceland stations, and surface waves, which are affected by a much wider area and therefore give the long-wavelength anisotropy, are consistent, indicating that the anisotropy pattern is similar over a wide area around Iceland.

Li and Detrick (2003) examined the phase velocities of Rayleigh waves recorded at stations across Iceland and constructed 2D phase velocity maps for different periods in the range of 25–67 s. They found that for surface waves in the period range of 50–67 s, which are mostly affected by the Earth structure between about 50 and 100 km depth, the fast directions are in the NW–SE direction in the central and east Iceland, again in agreement with the results presented here.

The global tomography results of Ekström (2001) also give a similar fast propagation directions in the Iceland area for Rayleigh waves of period 50–150 s.

7. Conclusions

Presented in this paper is a 3D S_v -wave velocity and azimuthal anisotropy model for the upper mantle beneath the North Atlantic and surrounding regions

derived from the analysis of about 9000 multi-mode Rayleigh-wave seismograms. This is a model of higher resolution than the one previously constructed from a subset of this data (Pilidou et al., 2004), but the main features of the two models are similar. The dense path coverage, the wide azimuthal distribution and the substantial higher-mode content of the dataset as well as the short path-lengths in the dataset have enabled us to build an upper mantle model for the region with a horizontal resolution of a few hundred kilometers extending to 400 km depth. The extensive testing carried out with a subset of the data (Pilidou et al., 2004) demonstrates that good resolution is achieved both laterally, due to dense ray coverage and good azimuthal coverage, and vertically, due to multi-mode analysis and a wide frequency range. However, because of the uneven distribution of higher modes, depth resolution is better in central Europe than in the central North Atlantic Ocean.

Low-velocity anomalies occur in the upper mantle beneath three major hotspots existing in the area: Eifel, Iceland and the Azores. The Eifel hotspot is located in NW Europe where the model has the best depth resolution. This low-velocity feature extends to the bottom of the model at 400 km depth. Iceland is located on the mid-Atlantic Ridge and the Azores are located near the ridge. The upper mantle low-velocity anomalies beneath both these hotspots are elongated in the direction of the ridge and extend to about 200 km depth. No low-velocity features were found that might be interpreted as plume stems beneath these oceanic hotspots. However, this doesn't rule out the existence of plume stems, as such narrow features (~200 km) are not expected to be properly resolved in the deep part of the model.

Our model shows a low-velocity structure, centered on Iceland with S_v -wave speeds -4% to -7% slow with respect to PREM. At 75–125 km depth, it is elongated along the mid-Atlantic Ridge axis to the NE and SW of Iceland, with along-ridge and across-ridge dimensions of 1700 and 600 km, respectively. At 150 km depth, the anomaly is strongest in the SW of Iceland, where it is approximately circular with a diameter of about 1000 km. There are a number of geophysical and geochemical observations indicating the flow of plume material along the Reykjanes Ridge south of Iceland, in agreement with the tomographic

model presented here. The structure of this model agrees with numerical models related to buoyancy-upwelling and flow of the plume mantle material along the ridge. The low-velocity anomaly extends to the north of Iceland beneath the Kolbeinsey Ridge, where there is weaker supporting evidence for the flow of plume material along the ridge. This low-velocity feature, however, might additionally be associated with a plume beneath Jan Mayen.

The anomaly associated with the Azores is -4% to -7% slow with respect to PREM at 75–150 km depth and extends from about 25°N to 45°N along the ridge axis. Compared to the anomaly associated with Iceland, the Azores anomaly is elongated further along the ridge, is shallower and decays more rapidly with depth. Geophysical as well as geochemical observations indicate that the Azores Plume influences the ridge between 27°N and 44°N , which is consistent with the seismic anomaly that observed here. The Azores Plume thermal anomaly is expected to be weaker than that of the Iceland Plume, implying a higher viscosity for which 3D numerical modelling experiments predict a shallower anomaly, consistent with our observations. Both the higher ridge-spreading rate and the higher viscosity of the Azores Plume suggest a smaller along-axis width than the corresponding width of the Iceland anomaly. This is inconsistent with our observations. However, the ridge spreads obliquely in the Azores region and this may tend to increase the along-axis width of the anomaly.

The third low-velocity anomaly is associated with the Eifel hotspot in NW Europe, which is an area of best ray density, azimuthal coverage and, hence, resolution. Unlike the Iceland and Azores anomalies, this anomaly extends to 400 km depth and, as expected for an intraplate plume, it is not elongated in any preferred direction. At shallow depth (75–100 km), it is 4–5% slow with respect to PREM and weakens to about -2% deeper, except for a thin zone between 150 and 250 km where it strengthens to about -3% . The small lateral extent of the plume head and the smaller total erupted volume of volcanic material may result from a smaller total heat flux plume trapped beneath a thicker continental plate. In this case, the degree of decompression melting in the Eifel Plume would be small compared to the degree of decompression melting of the higher heat flux Icelandic Plume beneath the thin oceanic plate.

The fast propagation direction in the asthenosphere (150–300 km depth) in the ocean south of Iceland correlates well with the E–W plate motion and the ridge-spreading direction. In the vicinity of Iceland, the direction changes to NW–SE, and is in agreement with the results of shear-wave splitting measurements across Iceland of Bjarnason et al. (1996, 2002) and Li and Detrick (2003), the regional tomographic study of Li and Detrick (2003) and the global tomography results of Ekström (2001).

Acknowledgements

We would like to thank Haukur Brynjólfsson at the University of Iceland Science Institute for his help with seismometer installation and service in East Greenland. We thank James McKenzie, Chris Lightfoot, Katy Raven and Jeff Parke for their assistance with seismometer installations in Scotland and Ireland. We thank Alex Brisbane and Jón Ásgeirsson for help with the instrument in Faroe Islands and Marin and Helge Nielsen for allowing us to use their facility to home an instrument. Special thanks to the staff of the Glenveigh National Park (Ireland) for their assistance during the seismometer installation in Ireland and Thomas Rasmussen and staff at the Sirius Patrol at Daneborg, NE Greenland, for their help with operating an instrument there. Thanks to Birgir Bjarnason and family for letting us use their farmhouses at Middalur for one of our instruments, and to Bob Watters for kindly allowing us to install a seismometer on his property as well as providing accommodation during the installation at the Isle of Skye. Instruments for the stations we deployed were supplied by SEIS-UK. We thank the IRIS and GEOSCOPE teams for providing data from the permanent stations. Part of the data from non-permanent stations came from the Geofon Data Centre, the AWE Blacknest Seismology group, the Canadian National Seismological Data Centre, the Norwegian Institute of Solid Earth Physics group and the Danish National Survey, Cadastre group and KMS stations in Denmark and Greenland. We thank Gunnar Gudmundsson for supply of data from the Sil network in Iceland and to Reynir Bödvarsson for supply of data from the Uppsala Network in Sweden. Data was also used from the HOTSPOT and ICEMELT networks in Iceland. Finally, we would like to acknowledge

financial support from the Cambridge Commonwealth/ Overseas Trust, the Danish Lithosphere Center and the A.G. Leventis Foundation. All maps were created with the Generic Mapping Tools (GMT) data processing and display package. This is University of Cambridge, Department of Earth Sciences, contribution 7911.

References

- Alber, M., Christensen, U.R., 2001. Channeling of plume flow beneath mid-ocean ridges. *Earth Planet. Sci. Lett.* 187, 207–220.
- Allen, R.M., Nolet, G., Jason Morgan, W., Vogfjörð, K., Bergsson, B.H., Erlendsson, P., Foulger, G.R., Jakobstóttir, S., Julian, B.R., Pritchard, M., Ragnarsson, S., Stefánsson, R., 1999. The thin hot plume beneath Iceland. *Geophys. J. Int.* 137, 51–63.
- Allen, R.M., Nolet, G., Jason Morgan, W., Vogfjörð, K., Bergsson, B.H., Erlendsson, P., Foulger, G.R., Jakobstóttir, S., Julian, B.R., Pritchard, M., Ragnarsson, S., Stefánsson, R., 2002a. Imaging the mantle beneath Iceland using integrated seismological techniques. *J. Geophys. Res.* 107 (B12).
- Allen, R.M., Nolet, G., Jason Morgan, W., Vogfjörð, K., Nettles, M., Ekström, G., Gergsson, B.H., Erlendsson, P., Foulger, G.R., Jakobstóttir, S., Julian, B.R., Pritchard, M., Ragnarsson, S., Stefánsson, R., 2002b. Plume driven plumbing and crustal formation in Iceland. *J. Geophys. Res.* 7 (B8).
- Bassin, C., Laske, G., Masters, G., 2000. The current limits of Resolution for surface wave tomography in North America. *EOS Trans. AGU* 81, 897.
- Bijwaard, H., Spakman, W., 1999. Tomographic evidence for a narrow whole mantle plume below Iceland. *Earth Planet. Sci. Lett.* 166, 121–126.
- Bjarnason, I.Th., Menke, W., Flóvenz, O., Caress, D., 1993. Tomographic image of the spreading center in southern Iceland. *J. Geophys. Res.* 98, 6607–6622.
- Bjarnason, I.Th., Wolfe, C.J., Solomon, S.C., 1996. Initial results from the ICEMELT experiment: body-wave delay times and shear-wave splitting across Iceland. *J. Geophys. Res.* 23 (5), 459–462.
- Bjarnason, I.Th., Silver, P.G., Rumpker, G., Solomon, S.C., 2002. Shear wave splitting across the Iceland hotspot: results from the ICEMELT experiment. *J. Geophys. Res.* 107 (B12), 2382.
- Cara, M., Lévêque, J.J., 1987. Waveform inversion using secondary observables. *Geophys. Res. Lett.* 14, 1046–1049.
- Darbyshire, F.A., Priestley, K.F., White, R.S., Stefánsson, R., Gudmundsson, G.B., Jakobsdóttir, S.S., 2002a. Crustal structure of central and northern Ireland from analysis of teleseismic receiver functions. *Geophys. J. Int.* 143 (1), 163–184.
- Darbyshire, F.A., White, R.S., Priestley, K.F., 2002b. Structure of the crust and uppermost mantle of Iceland from a combined seismic and gravity study. *Earth Planet. Sci. Lett.* 181 (3), 409–428.
- Debayle, E., 1999. SV-wave azimuthal anisotropy in the Australian upper mantle: preliminary results from automated Rayleigh waveform. *Geophys. J. Int.* 137, 747–754.
- Debayle, E., Lévêque, J.-J., Cara, M., 2001. Seismic evidence for a plume in the upper mantle beneath the northeastern Afro/Arabian continent. *Earth Planet. Sci. Lett.* 193, 423–436.
- Debayle, E., Kennett, B.L.N., 2000. Anisotropy in the Australasian upper mantle from Love and Rayleigh waveform inversion. *Earth Planet. Sci. Lett.* 184, 339–351.
- Dosso, L., Bougault, H., Joron, J.-L., 1993. Geochemical morphology of the North Mid-Atlantic Ridge, 10°–24°N: trace element-isotope complementary. *Earth Planet. Sci. Lett.* 120, 443–462.
- Dziewonski, A.M., Anderson, D.L., 1981. Preliminary reference earth model. *Phys. Earth Planet. Inter.* 25 (4), 297–356.
- Ekström, G., 2001. Mapping azimuthal anisotropy of intermediate-period surface waves (abstract). *EOS Trans. AGU* 82 (47) (S51E–06).
- Faccenna, C., Jolivet, L., Piromallo, C., Morelli, A., 2003. Subduction and the depth of convection in the Mediterranean mantle. *J. Geophys. Res.* 108 (ETG9-1/13).
- Fitton, J.G., Saunders, A.D., Norry, M.J., Hardarson, B.S., Taylor, R.N., 1997. Thermal and chemical structure of the Iceland plume. *Earth Planet. Sci. Lett.* 153, 197–208.
- Foulger, G.R., Pritchard, M.J., Julian, B.R., Evans, J.R., Allen, R.M., Nolet, G., Morgan, W.J., Bergsson, B.H., Erlendsson, P., Jakobstóttir, S., Ragnarsson, S., Stefánsson, R., Vogfjörð, K., 2001. Seismic tomography shows that upwelling beneath Iceland is confined to the upper mantle. *Geophys. J. Int.* 146, 504–530.
- Gaherty, J.B., 2001. Seismic evidence for hotspot-induced buoyant flow beneath the Reykjanes Ridge. *Science* 293, 1645–1647.
- Goslin, J., Triatnord Scientific Party, 1999. Extent of Azores plume influence on the Mid-Atlantic Ridge north of the hotspot. *Geophys. J. Int.* 27 (11), 991–994.
- Goslin, J., Thiro, J.-L., Noel, O., Francheteau, J., 1998. Slow-ridge/hotspot interactions from global gravity, seismic tomography and ⁸⁷Sr/⁸⁶Sr isotope data. *Geophys. J. Int.* 135, 700–710.
- Griesshaber, E., O’Nions, R.K., Oxburgh, E.R., 1992. Helium and carbon isotope systematics in crustal fluids from the Eifel, the Rhine Graben and the Black Forest, FRG. *Chem. Geol.* 99, 213–235.
- Helmberger, D.V., Wen, L., Ding, X., 1998. Nature of the crust mantle transition zone and the thermal state of the upper mantle beneath Iceland from gravity modelling. *Nature* 396, 251–255.
- Hoernle, K., Zhang, Y.-S., Graham, D., 1995. Seismic and geochemical evidence for large-scale mantle upwelling beneath the eastern Atlantic and western and central Europe. *Nature* 374, 34–39.
- Ito, G., Lin, J., 1995. Oceanic spreading center–hotspot interactions: constraints from along-isochron bathymetric and gravity anomalies. *Geology* 23, 657–660.
- Jones, S., White, N., MacLennan, J., 2002. V-shaped ridges around Iceland: implications for spatial and temporal patterns of mantle convection. *Geochem. Geophys. Geosyst.* 3, 1059. (2002GC000361).
- Keller, W.R., Anderson, D.L., Clayton, R.W., 2000. Resolution of tomographic models of the mantle beneath Iceland. *Geophys. Res. Lett.* 27, 3993–3996.
- Kennett, B.L.N., 1995. Approximations for surface-wave propagation in laterally varying media. *Geophys. J. Int.* 122, 470–478.

- Keyser, M., Ritter, J.R.R., Jordan, M., 2002. 3D shear-wave velocity structure of the Eifel plume, Germany. *Earth Planet. Sci. Lett.* 203, 59–82.
- Lévêque, J.-J., Cara, M., Rouland, D., 1991. Waveform inversion of surface wave data: test of a new tool for systematic investigation of upper mantle structure. *Geophys. J. Int.* 104, 518–565.
- Lévêque, J.J., Debayle, E., Maupin, V., 1998. Anisotropy in the Indian Ocean upper mantle from Rayleigh and Love waveform inversion. *Geophys. J. Int.* 133, 529–540.
- Li, A., Detrick, R.S., 2003. Azimuthal anisotropy and phase velocity beneath Iceland: implication for plume–ridge interaction. *Earth Planet. Sci. Lett.* 6763, 1–13.
- Marquering, H., Snieder, R., 1996. Shear-wave velocity structure beneath Europe, the northeastern Atlantic and western Asia from waveform inversion including surface-wave mode coupling. *Geophys. J. Int.* 127, 283–304.
- Marquering, H., Snieder, R., Nolet, G., 1996. Waveform inversion and the significance of surface-wave mode coupling. *Geophys. J. Int.* 124, 258–278.
- McKenzie, D., 1984. Generation and compaction of partial molten rock. *J. Petrol.* 25, 713–765.
- Montagner, J.P., 1986. Regional three-dimensional structures using long-period surface waves. *Ann. Geophys.* 4, 283–294.
- Montagner, J.P., Ritsema, J., 2001. Interactions between ridges and plumes. *Science* 294, 1472–1473.
- Nataf, H.-C., Ricard, Y., 1996. 3SMAC: an *a priori* tomographic model of the upper mantle based on geophysical modeling. *Phys. Earth Planet. Inter.* 95, 101–122.
- Nishimura, C.E., Forsyth, D.W., 1989. The anisotropic structure of the upper mantle in the Pacific. *Geophys. J. Int.*, 203–229.
- Pilidou, S., Priestley, K., Gudmundsson, Ó., Debayle, E., 2004. Upper mantle S-wave speed heterogeneity beneath the North Atlantic and the surrounding region from regional surface wave tomography. *Geophys. J. Int.* (to appear).
- Priestley, K., Debayle, E., 2003. Seismic evidence for a moderately thick lithosphere beneath the Siberian Platform. *Geophys. Res. Lett.* 30 (3).
- Priestley, K., Tilmann, F., 1999. Shear-wave structure of the lithosphere above the Hawaiian hotspot from two-station Rayleigh wave phase velocity measurements. *Geophys. Res. Lett.* 26, 1493–1496.
- Ritsema, J., Allen, R.M., 2003. The elusive mantle plume. *Earth Planet. Sci. Lett.* 207, 1–12.
- Ritsema, J., van Heijst, H.J., Woodhouse, J.H., 1999. Complex shear wave velocity structure imaged beneath Africa and Iceland. *Science* 286, 1925–1928.
- Ritter, J.R.R., Jordan, M., Christensen, U.R., Achauer, U., 2001. Mantle plume below the Eifel volcanic fields, Germany. *Earth Planet. Sci. Lett.* 186, 7–14.
- Schilling, J.G., 1973. Iceland mantle plume: geochemical study of Reykjanes Ridge. *Nature* 242, 65–571.
- Schilling, J.G., 1985. Upper mantle heterogeneities and dynamics. *Nature* 314, 65–67.
- Schilling, J.G., 1991. Fluxes and excess temperatures of mantle plumes inferred from their interaction with migrating mid-ocean ridges. *Nature* 352, 397–403.
- Schilling, J.G., Kingsley, R., Fontignie, D., Poreda, R., Xue, S., 1999. Dispersion of the Jan Mayen and Iceland mantle plumes in the Arctic: a He–Pb–Nd–Sr isotope tracer study of basalts from the Kolbeinsey, Mohs and Knipovich Ridges. *J. Geophys. Res.* 10 (5), 10543–10569.
- Searle, R.C., Keeton, J.A., Owens, R.B., White, R.S., Mecklenburgh, R., Parsons, B., Lee, S.M., 1998. The Reykjanes Ridge: structure and tectonics of a hot-spot-influenced, slow-spreading ridge, from multibeam bathymetry, gravity and magnetic investigations. *Earth Planet. Sci. Lett.* 160, 463–478.
- Shen, Y., Solomon, S.C., Bjarnason, I.Th., Purdy, G.M., 1996. Hot mantle transition zone beneath Iceland and the adjacent Mid-Atlantic Ridge inferred from P-to-S conversions at the 410- and 660-km discontinuities. *Geophys. Res. Lett.* 23, 3527–3530.
- Shen, Y., Solomon, S.C., Bjarnason, I.Th., Wolfe, C.J., 1998. Seismic evidence for a lower mantle origin of the Iceland mantle plume. *Nature* 395, 62–65.
- Sleep, N.H., 1990. Hotspots and mantle plumes: some phenomenology. *J. Geophys. Res.* 95, 6715–6736.
- Smallwood, R., White, R.S., 1998. Crustal accretion at the Reykjanes Ridge, 61°–62°N. *J. Geophys. Res.* 103, 5185–5201.
- Staples, R., White, R., Brandsdóttir, B., Menke, W., Maguire, P., McBride, J., Smallwood, J., 1997. Faeroe-Iceland Ridge Experiment: I. The crustal structure of north-eastern Iceland. *J. Geophys. Res.* 102, 7849–7866.
- Taylor, R.N., Thirlwall, M.F., Murton, B.J., Hilton, D.R., Gee, M.A.M., 1993. Isotopic constraints on the influence of the Icelandic plume. *Earth Planet. Sci. Lett.* 148, E1–E8.
- Thibaud, R., Gente, P., Maia, M., 1997. A systematic analysis of the Mid-Atlantic Ridge morphology and gravity between 15°N and 40°N. *J. Geophys. Res.* 103 (B10), 24223–24243.
- Tryggvason, E., Husebye, E.S., Stefánsson, R., 1983. Seismic image of the hypothesized Icelandic hotspot. *Tectonophysics* 100, 97–118.
- Vogt, P.R., 1971. Asthenosphere motion recorded by the ocean floor south of Iceland. *Earth Planet. Sci. Lett.* 13, 153–160.
- Wolfe, C.J., Bjarnason, I.Th., VanDecar, J.C., Solomon, S.C., 1997. Seismic study of the Iceland mantle plume. *Nature* 385, 245–247.
- Yoshizawa, K., Kennett, B.L.N., 2002. Determination of the influence zone for surface wave paths. *Geophys. J. Int.* 149, 440–453.
- Zhang, Y.S., Lay, T., 1999. Evolution of oceanic upper mantle. *Phys. Earth Planet. Inter.* 114, 71–80.
- Zhao, D., 2001. Seismic structure and origin of hotspots and mantle plumes. *Earth Planet. Sci. Lett.* 192, 251–265.
- Zielhuis, A., Nolet, G., 1994. Shear wave velocity variations in the upper mantle beneath central Europe. *Geophys. J. Int.* 117, 695–715.